

CBF, BOLD, CBV, and CMRO₂ fMRI Signal Temporal Dynamics at 500-msec Resolution

Qiang Shen, PhD, Hongxia Ren, PhD, and Timothy Q. Duong, PhD*

Purpose: To investigate the temporal dynamics of blood oxygenation level-dependent (BOLD), cerebral blood flow (CBF), cerebral blood volume (CBV), and cerebral metabolic rate of oxygen (CMRO₂) changes due to forepaw stimulation with 500-msec resolution in a single setting.

Materials and Methods: Forepaw stimulation and hypercapnic challenge on rats were studied. CBF and BOLD functional MRI (fMRI) were measured using the pseudo-continuous arterial spin-labeling technique at 500-msec resolution. CBV fMRI was measured using monocrySTALLINE iron-oxide particles following CBF and BOLD measurements in the same animals. CMRO₂ change was estimated via the biophysical BOLD model with hypercapnic calibration. Percent changes and onset times were analyzed for the entire forepaw somatosensory cortices and three operationally defined cortical segments, denoted Layers I–III, IV–V, and VI.

Results: BOLD change was largest in Layers I–III, whereas CBF, CBV, and CMRO₂ changes were largest in Layers IV–V. Among all fMRI signals in all layers, only the BOLD signal in Layers I–III showed a poststimulus undershoot. CBF and CBV dynamics were similar. Closer inspection showed that CBV increased slightly first ($P < 0.05$), but was slow to peak. CBF increased second, but peaked first. BOLD significantly lagged both CBF and CBV ($P < 0.05$).

Conclusion: This study provides important temporal dynamics of multiple fMRI signals at high temporal resolution in a single setting.

Key Words: hemodynamic coupling; brain mapping; cerebral blood flow; cerebral blood volume

J. Magn. Reson. Imaging 2008;27:599–606.
© 2008 Wiley-Liss, Inc.

basis for many modern neuroimaging modalities, including positron emission tomography, intrinsic optical imaging, and functional MRI (fMRI). Following stimulus-evoked changes in neural activity, cerebral blood flow (CBF), cerebral blood volume (CBV), and oxygenation in different vascular compartments change with different spatial and temporal dynamics. These hemodynamic changes coupled with oxygen metabolic changes give rise to the blood oxygenation level-dependent (BOLD) signals (2). The precise temporal dynamics (such as onset times and times to peak) and spatial dynamics (such as arterioles, capillaries, and venules) of these fMRI signals remain an active area of research (3–6).

Combined intrinsic optical imaging and laser Doppler flow (7) techniques can dynamically measure stimulus-evoked changes in CBF, CBV, and deoxyhemoglobin concentration on the cortical surfaces at very high temporal resolution. The deoxyhemoglobin optical signal had been consistently shown to precede CBF, CBV, and oxyhemoglobin signals (8–10). Reports of relative CBV and CBF dynamics have been controversial. Malonek et al. (8) reported that CBV increased before CBF, whereas Sheth et al. (11) reported CBV lagged CBF and Jones et al. (9,10) reported CBV and CBF had similar onset times and times to peak.

Functional MRI signals measuring CBV and CBF changes also show similar controversy, although the literature is sparse, limited by the low temporal resolution of current CBF MRI techniques. Stimulus-evoked CBV onset, measured using the monocrySTALLINE iron-oxide nanocalloid (MION) MRI contrast agent, has been reported to lag BOLD onset in a rat forepaw stimulation model under α -chloralose anesthesia (12), whereas CBV onset precedes the BOLD onset in the same rat model (13). The typical temporal resolution of CBF fMRI is a few seconds, insufficient to resolve differences in CBF and CBV temporal dynamics. High temporal resolution measurements of CBF, CBV, and BOLD fMRI in the same pixels in a single setting could therefore offer the potential to resolve this inconsistency as well as provide a better understanding of the temporal dynamics of these hemodynamic responses. Moreover, CBF, CBV, and BOLD fMRI offer the opportunity to investigate layer-specific-dependent effects that are not feasible with optical imaging techniques.

THE INTRICATE NEURAL-VASCULAR COUPLING (1) associated with changes in neural activity forms the

Department of Neurology and Radiology, Yerkes Imaging Center, Division of Neuroscience, Yerkes National Primate Research Center, Emory University, Atlanta, Georgia.

Contract grant sponsor: Scientist Development Grant from the American Heart Association; Contract grant number: SDG-0430020N; Contract grant sponsor: National Institutes of Health; Contract grant number: R01-NS45879.

*Address reprint requests to: T.Q.D., PhD, Yerkes Imaging Center, Emory University, 954 Gatewood Rd. NE, Atlanta, GA 30329. E-mail: tduong@emory.edu

Received March 25, 2007; Accepted September 5, 2007.

DOI 10.1002/jmri.21203

Published online 24 January 2008 in Wiley InterScience (www.interscience.wiley.com).

In this study we implemented BOLD, CBF, and CBV fMRI measurements in a single setting with a 500-msec temporal resolution. Rat forepaw stimulation under isoflurane anesthesia was used in which the animals breathed spontaneously and autoregulated their own physiology over a relatively long time (as opposed to mechanical ventilation, which requires frequent blood-gas sampling) (14–16). High temporal resolution CBF fMRI was made possible by using the pseudo-continuous arterial spin-labeling technique (17) where labeled and nonlabeled time-series images were acquired sequentially instead of in a pairwise fashion. BOLD signal was taken from the nonlabeled images of the CBF measurements. CBV fMRI was measured using MION following CBF and BOLD measurements in the same animals. Changes in the cerebral metabolic rate of oxygen (CMRO₂) were estimated using Davis' biophysical BOLD model with hypercapnic calibration (14,18,19). fMRI signal percent changes, onset times, and poststimulus undershoots were analyzed for the entire forepaw somatosensory cortices and for three operationally defined cortical layers denoted Layers I–III, IV–V, and VI.

MATERIALS AND METHODS

Animal Preparation

Eight male Sprague-Dawley rats (300–375 g) were anesthetized with 2% isoflurane during placement of a femoral vein catheter for MION injection (14 mg/kg) and stimulation needle electrodes under the forepaw skin. This MION dosage is sufficient to yield negligible BOLD contributions (20,21). Rats were secured in an MR-compatible rat stereotaxic headset. Isoflurane was reduced to 1.1% to 1.2% during MRI. The forepaw stimulation model using isoflurane had been described and discussed in detail elsewhere (14,15) and recently replicated by others, albeit with slightly different stimulation parameters (22). Rats breathed spontaneously without mechanical ventilation. One advantage of this preparation is that all animals were able to maintain their physiological parameters (blood gases, respiration, and heart rates and oxygen saturation) as documented previously under normal conditions (14, 15, 22) and cerebral ischemia (16). Oxygenation saturation, respiration rate, heart rate, and rectal temperature were monitored and maintained within physiological ranges, but invasive blood-gas sampling was not used.

Hypercapnic Challenge and Forepaw Stimulation

Hypercapnic challenge (5% CO₂ in air) was used for calibration to estimate CMRO₂ change associated with the forepaw stimulation (14,18). Hypercapnic challenge consisted of 120 seconds of baseline condition followed by 120 seconds of hypercapnia. For forepaw somatosensory stimulation, needle electrodes were inserted under the skin of the left and right forepaw, such that both forepaws were stimulated simultaneously in series at a constant current. The stimulation current was 6 mA with 0.3 msec pulse duration at 3 Hz as optimized previously for this model (14). These stimulation parameters had twice the current but three times shorter pulse duration than a recent report using isoflurane

anesthesia (22). The forepaw stimulation consisted of 3 epochs of 60 seconds OFF and 20 seconds ON. Two to three repeated trials were made on each animal. Breaks of at least 15 minutes were given between trials.

MRI Experiments

MRI experiments were performed on a 4.7T/40-cm magnet, a Biospec Bruker console (Billerica, MA), and a 20-G/cm gradient insert (ID = 12 cm, 120- μ s rise time). A surface coil (2.3-cm ID) was used for brain imaging and a neck coil (23) for arterial spin labeling. Coil-to-coil electromagnetic interaction was actively decoupled. High-resolution anatomical images were acquired using the fast spin-echo pulse sequence with TR = 2 seconds (90° flip angle), 16 echo trains, effective TE = 104 msec, matrix = 128 \times 128, FOV = 2.56 cm \times 2.56 cm, two 2-mm slices, and 16 averages.

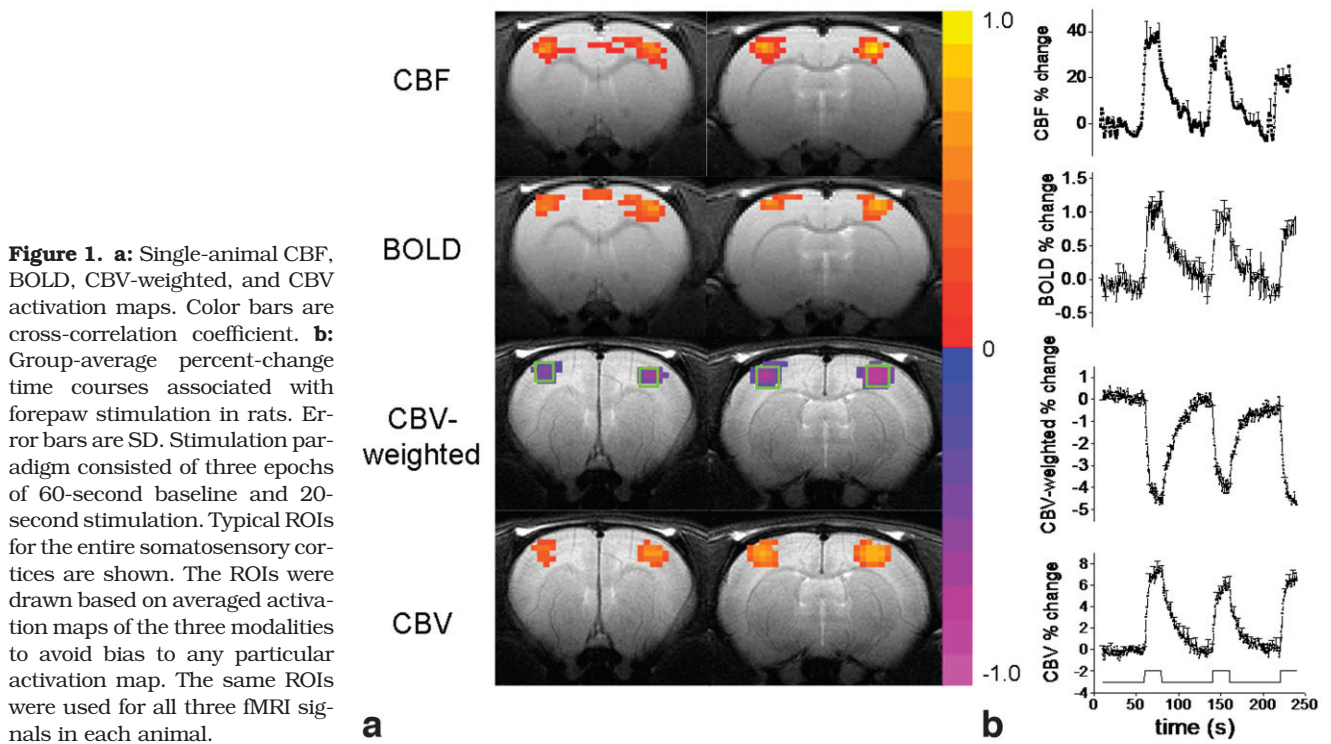
To achieve high temporal resolution, CBF measurements were made using the pseudo-continuous arterial spin-labeling technique (17) with single-shot, gradient-echo, echo-planar-imaging (EPI) acquisition. MRI parameters were: labeling duration = 416 msec, data matrix = 64 \times 64, FOV = 2.56 cm \times 2.56 cm, two 2.0-mm slices, TE = 16 msec, and TR = 500 msec. An Ernst flip angle was used to minimize in-flow effect. Time series of labeled and nonlabeled images were acquired consecutively in two separate scans (not in pairs). The nonlabeled images were taken as BOLD images. A relatively short TE was chosen to increase CBF signal-to-noise ratio (SNR) to approximate the BOLD SNR in the combined CBF and BOLD measurements. While the BOLD data at such short echo time could accentuate the blood signal, as this is very near the blood T2*, it is not expected to significantly compromise the temporal dynamics and our conclusions. Continuous arterial spin labeling was employed in the presence of 1.0 G/cm gradient along the flow direction for adiabatic inversion. The sign of the frequency offset was switched for nonlabeled images.

After forepaw stimulation and hypercapnic BOLD and CBF measurements, MION was injected and CBV fMRI were measured associated with forepaw stimulation. The MRI parameters were identical to those of the CBF measurements except only the nonlabeled images were acquired.

Data Analysis

Data analysis employed codes written in Matlab (MathWorks, Natick, MA) and the STIMULATE software (University of Minnesota). CBV-weighted and CBV images were determined at each timepoint based on Ref. 12. BOLD images were obtained from the nonlabeled images of the CBF measurements. CBF images (S_{CBF}) with intensities in ml/g/min were calculated at each timepoint (23). Subtraction of non-labeled and labeled images in the CBF measurement is expected to remove essentially all BOLD contributions from the CBF signal.

The pseudo-continuous arterial spin-labeling technique (17) resulted in mixing of CBF changes and T1 effect which needed to be deconvolved. Deconvolution was applied on the CBF time courses to remove the T1



effect in which the time constant was obtained from the first few timepoints of the MRI measurements. The temporal deconvolution of the CBF time course was performed using a polynomial fit constrained from 1 to 20 seconds following the stimulation onset. No assumption was made regarding the hemodynamic response function.

CMRO₂ Calculation

CMRO₂ changes were calculated from the average of BOLD, CBF, and CBV time courses by using the biophysical BOLD model (18, 19, 24):

$$\frac{\Delta BOLD}{BOLD_0} = M \left(1 - \left(\frac{CMRO_2}{CMRO_{2,0}} \right)^\beta \left(\frac{CBV}{CBV_0} \right) \left(\frac{CBF}{CBF_0} \right)^{-\beta} \right) \quad (1)$$

Conversion of CBV/CBV₀ to CBF/CBF₀ via Grubb's factor was not necessary because CBV/CBV₀ was measured (18,19,24). The proportionality constant M relating BOLD, CBF, and CBV changes reflects the maximum BOLD response that can be expected from a given region; the measured group-average M value in the forepaw somatosensory cortices from the hypercapnic data was used (see Results). β is the proportionality constant relating deoxyhemoglobin concentration to the BOLD signals and a value of 1.5 was used (18,25). The effects of different constants on the CMRO₂ calculation and uncertainties of CMRO₂ estimations have been addressed and Monte Carlo simulations showed that CMRO₂ are weakly dependent on these constants over the physiological ranges (14,18,19).

Percent Change Analysis

Region of interest (ROI) analysis of percent changes was performed. To minimize bias in the ROI analysis, the

BOLD, CBF, and CBV cross-correlation maps were averaged and ROIs enclosing the primary somatosensory cortices (≈ 9 pixels, as shown in Fig. 1) were carefully drawn on the averaged fMRI maps with reference to anatomical images. Percent changes of individual (BOLD, CBF, CBV, and CMRO₂) fMRI signals in each animal were obtained from the same ROIs. In addition, ROI analysis was also performed on three operationally defined layers (Layers I-III, IV-V, VI) within the forepaw somatosensory cortices as shown in Fig. 4, similar to the definition employed previously (26).

Time courses were first averaged across repeated measures, left and right primary somatosensory cortex. CBF time courses were deconvolved before averaging across animals.

Onset Times and Times to Peak

Percent changes and normalized percent changes were plotted. Normalized percent changes from 0 to 1 allowed fair comparison of onset times and times to peak among signals that have very different percent changes. Onset time was defined at 30% of maximum. The time to peak was defined as 90% of maximum. Percent changes, onset times, and times to peak were tabulated. Values in the text are mean \pm SD and values in the graphs were SEM for $n = 8$ rats. A paired *t*-test was used to test for statistical differences.

RESULTS

For hypercapnic (5% CO₂) challenge, the group-average BOLD and CBF percent changes were $4.9 \pm 0.1\%$ and $114 \pm 54\%$, respectively. The group-average M value in the entire forepaw somatosensory cortices was $0.12 \pm$

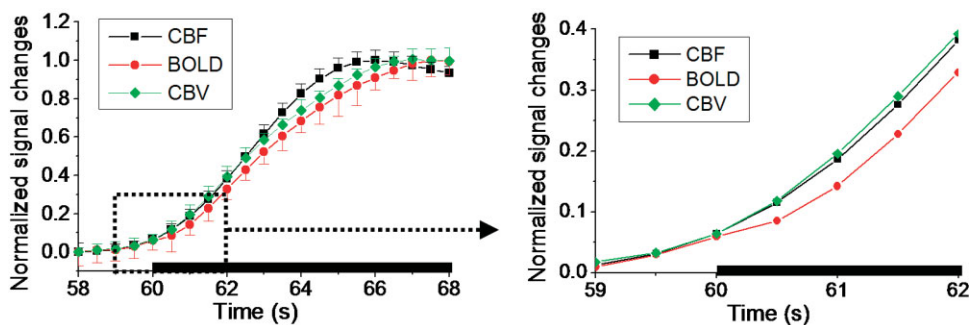


Figure 2. Normalized percent changes of CBF, BOLD, and CBV group-average time courses. Three epochs were averaged together to form one epoch. Error bars are standard error of the means ($n = 8$). Error bars in the expanded view are not shown for clarity.

0.03, which was used in the $CMRO_2$ calculations (M values across these three operationally defined layers were not statistically different).

CBF, CBV, and BOLD activation maps of bilateral forepaw stimulations from a representative animal are shown in Fig. 1a. The group-average percent-change time courses are shown in Fig. 1b. The average CBF, BOLD, and CBV percent changes were $37 \pm 11\%$, $1.1 \pm 0.3\%$, and $6.4 \pm 2.0\%$, respectively. Figure 2 shows the normalized CBF, BOLD, and CBV time courses of the forepaw stimulations, with the expanded time courses showing the detailed onset times. Although the CBF and CBV temporal dynamics were quite similar, there was a trend that CBV increased first but grew slower over time relative to CBF. CBF started out slightly later than CBV but peaked faster than CBV. The biggest difference between CBF and CBV onset time was at 30% of maximum ($P < 0.05$) and time to peak was at 90% of maximum ($P = 0.1$).

BOLD signal showed the slowest onset and peaked last, as expected, and its onset and time-to-peak were statistically different from those of the CBV ($P < 0.01$) and CBF ($P < 0.05$) signals. The group-average onset times and times to peak are summarized in Table 1 with comparison of data obtained from different laboratories. Note that the onset times and times to peak were not the multiple of 500 msec due to the averaging across multiple animals.

To investigate the laminar dependency of these fMRI signals, the group-average BOLD and $CMRO_2$ time courses from three operationally defined cortical segments, approximating Layers I-III, IV-V, and VI, are

plotted (Fig. 3). The largest BOLD changes were detected in Layers I-III. Only the BOLD time courses from Layers I-III showed a poststimulus undershoot. No poststimulus undershoot was observed for the $CMRO_2$ fMRI signals in any cortical layer. In fact, $CMRO_2$ appeared to remain slightly elevated in Layers IV-V and VI. CBV and CBF in all layers quickly returned to baseline poststimulus and no stimulus-undershoots were observed for CBV and CBF signals (data not shown). Quantitative percent changes of all fMRI signals in the three cortical segments are summarized in Fig. 4. The largest CBF, CBV, and $CMRO_2$ changes were detected in Layers IV-V, whereas the largest BOLD changes were detected in Layers I-III. The ratio of CBF: $CMRO_2$ change was 3:1 for Layers I-III and 2:1 for Layers IV-V and VI.

DISCUSSION

The major findings of this study are: 1) CBV and CBF dynamics are similar. Closer inspection revealed that, in the early phase, CBV increases slightly before CBF. 2) While CBF increases second, it overtakes CBV and peaks first, consistent with the notion that the arterial spin-labeling CBF technique is predominantly sensitive to changes in the arteriole compartment and is less sensitive to changes in large veins due to the loss of contrast associated with T1 recovery as spins traversed from the arteries to the draining veins. The slow-peaking CBV signal suggests increasing draining vein contribution during the steady-state phase. This biphasic CBV response is consistent with previous studies (12, 24). 3) The onset time and time to peak of the BOLD

Table 1
Group-Average Onset Times and Times to Peak (TTP) ($n = 8$ Rats, Two Paws per Rat)

	This study		Silva et al 2000 ^b		Silva et al 2004 ^c	
	Onset times ^a	TTP	Onset times	TTP	Onset times	TTP
CBF	1.7 ± 0.2 s**	4.5 ± 1.1 s	0.6 ± 0.4 s	4.5 ± 2.2 s	—	—
BOLD	2.0 ± 0.1 s	5.8 ± 2.6 s	1.1 ± 0.3 s	5.9 ± 3.8 s	~ 1.0 s	2.7 ± 0.6 s
CBV	1.4 ± 0.2 s***	5.0 ± 2.3 s	—	—	~ 0.7 s	1.9 ± 0.3 s

^aOnset times were obtained at 30% of maximum. Onset times obtained at 15% maximum showed similar results (not shown) but slightly more variable.

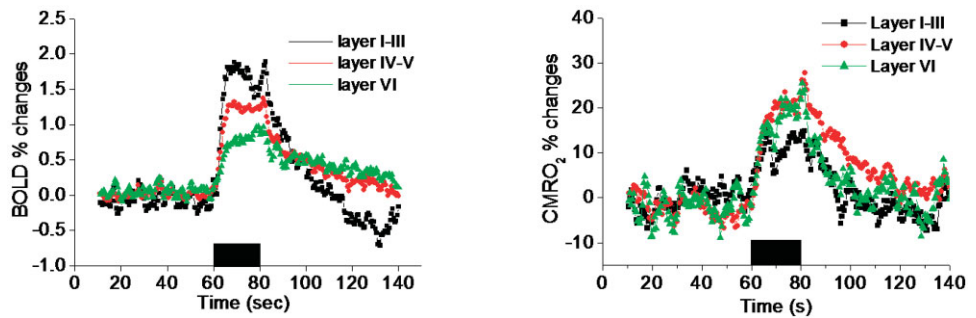
^bData were obtained from α -chloralose-anesthetized and mechanically ventilated rats at 9.4T. The stimulation duration was similar to this study (22 s) (20).

^cData were obtained from α -chloralose-anesthetized and ventilated rats at 11.7T where the stimulation duration was 0.5 s or 1 s (13). While absolute TTP values are dependent on stimulation duration as expected, the differences in TTP between BOLD and CBV (2.7 s $-$ 1.9 s = 0.8 s) is identical to this study (5.8 s $-$ 5.0 s = 0.8 s).

* $P < 0.05$: Onset times were significantly different from that of the CBF signals.

** $P < 0.01$: Onset times were significantly different from that of the BOLD signals.

Figure 3. Group-average percent changes of the BOLD and CMRO₂ time courses for three operationally defined cortical segments. Poststimulus BOLD undershoot was observed for Layers I-III. Poststimulus CMRO₂ was elevated in Layers IV-V and VI.



fMRI signal significantly lag those of CBF and CBV fMRI signals due to large venule and venous BOLD contribution, where the stimulus-evoked deoxyhemoglobin saturation changes are most pronounced. 4) The magnitudes of the fMRI signals are cortical-depth-dependent. The BOLD signal from the cortical surface (Layers I-III) shows the highest changes and only the BOLD signal from Layers I-III exhibits a poststimulus undershoot. In contrast, CBF and CBV fMRI signals show the largest changes in Layers IV-V and these signals showed no poststimulus undershoots. 5) The estimated CMRO₂ signals show the largest changes in Layers IV-V, consistent with being the most metabolically active layer. CMRO₂ remains slightly elevated poststimulus in Layers IV-V, and VI, but not Layers I-III, with no evidence of CMRO₂ poststimulus undershoot. While fMRI does not have sufficient spatial resolution to physically resolve different vascular compartments, the temporal latencies of the BOLD, CBF, and CBV fMRI signals could provide valuable information regarding their fMRI signal sources and their spatial specificity.

Potential Confounding Factors

There are a few factors and assumptions that could potentially confound the interpretation of these data. First, there could be an error associated with stimulus-evoked change in transit time, which affect the CBF value per se as well as deconvolution accuracy because CBF calculation did not take into account the stimulus-evoked changes in transit time. Measuring the mean transit time is difficult and is beyond the scope of this work. Second, to obtain the improved temporal resolution, labeled and nonlabeled images were acquired sequentially to achieve higher temporal resolution (as opposed to pairwise interleaved fashion) which could be more susceptible to intertrial variations of the forepaw fMRI responses. Third, isoflurane, a strong vasodilator, could cause sluggish blood flow changes and thus could affect the onset times and times to peak. Nonetheless, relative differences in onset times and times to peak among different fMRI signals should remain valid. Temporal dynamics under different anesthetics are under investigation. Fourth, three operationally defined

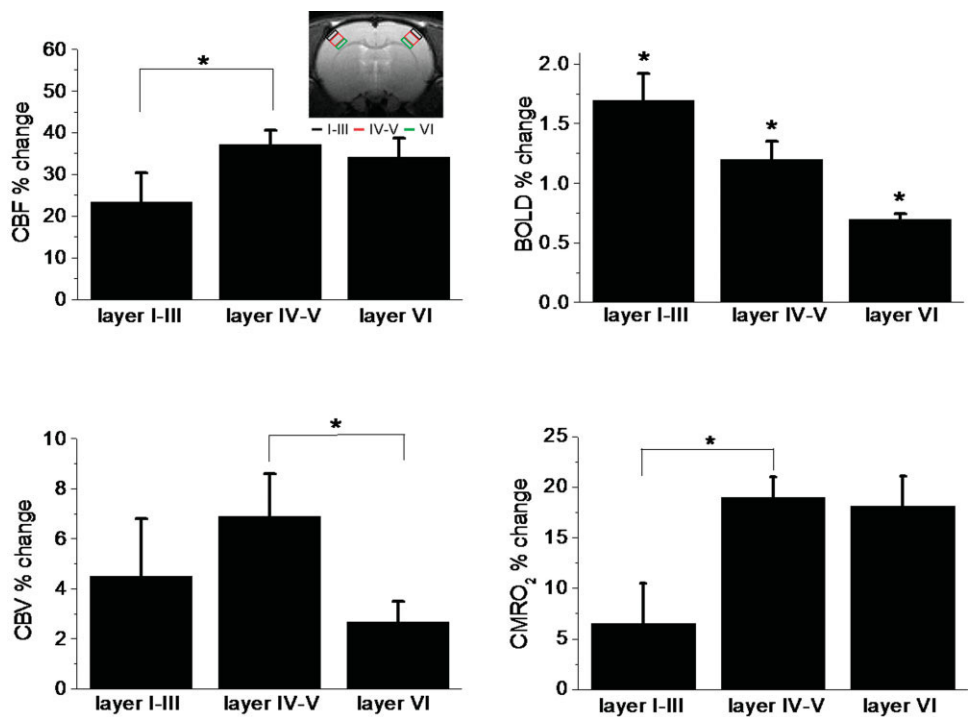


Figure 4. Group-average of CBF, BOLD, and CBV percent changes for three operationally defined cortical segments (Layers I-III, IV-V, VI). The inset shows the typical ROIs for the three operationally defined cortical layers. **P* < 0.05.

layers, similar to those defined by Silva et al. (26), were obtained to demonstrate layer-specific differences. The need for very high temporal resolution is unfortunately incompatible with the use of segmented EPI to increase spatial resolution. The spatial resolution herein, although typical, precluded the analysis of individual cortical layers and resulted in some partial-volume effects on the three operationally defined layers. Thus, caution must be exercised when interpreting these cortical layers. Improved spatial resolution would help to better distinguish cortical layers. Fifth, although there is a difference between CBF and CBV temporal dynamics, this difference is small and improved temporal resolution would be helpful. Jittered stimulus timing in which the stimulus is presented with different time delays within a TR (4) could also be used to achieve high temporal resolution but it is subject to intertrial errors.

Finally, $CMRO_2$ changes are estimates based on the biophysical BOLD model that assumes that CBF, CBV, and BOLD signals come from the same vascular sources and occur at the same time (valid for low spatial and temporal resolution data). While $CMRO_2$ changes taking into account different vascular contribution has been attempted (27), fitting a large number of parameters is susceptible to errors and additional assumptions need to be made. Given the small differences in both percent changes and temporal latencies, estimating the $CMRO_2$ change using the original Davis' biophysical model (18) appeared justified because at this spatial resolution a voxel contains a large mixture of different vessel sizes and types. Moreover, estimation of $CMRO_2$ using the biophysical model assumed that mild hypercapnia did not change oxygen metabolism, but this assumption has been questioned (28). Despite some shortcomings, Davis' biophysical BOLD model offers a means to gain insight into the dynamics of $CMRO_2$ changes associated with increased neural activities. A key contribution of this study is that CBF, CBV, BOLD, and $CMRO_2$ fMRI signals were obtained from the same ROIs in the same settings and using a single modality (MRI), in contrast to previous studies.

Cross-Laboratory Comparisons

The magnitudes of BOLD and CBF percent changes are consistent with those reported in the literature (20,21,24) and those reported previously using the same isoflurane-anesthetized forepaw stimulation model (14–16). CBV changes were slightly smaller than those reported previously (20,21). This is likely because of the differences in stimulus durations. In our study, CBV did not reach a plateau for our 20-second stimulation, whereas CBF and BOLD appeared to have reached the plateaus. This is interesting in and of itself and could be due to physiology of CBV response or the use of MION, requiring further investigation.

Although the difference was small, CBV onset was slightly earlier than the CBF onset during the early phase (at 30% of maximum, $P < 0.05$). This observation is consistent with that of Maloney et al. (8) but differs from that of Sheth et al. (11). Careful inspection of Jones et al.'s data (9,10) indicate that CBV also slightly precedes CBF at the early onset but slow to peak rela-

tive to the CBF signal, in good agreement with our data. Our results are also in good agreement with those reported by Huppert et al. (4), in which CBF was measured using ASL MRI with jittered stimulus presentations to achieve high temporal resolution and CBV was measured using near infrared spectroscopy. More recently, Vanzetta et al. (6) employed oxygen-sensitive fluorescent and intrinsic optical imaging to resolve different vascular compartments in terms of blood volume and oximetric changes. They found that vascular responses began at the arteriolar level rapidly spreading toward capillaries and venules. Our data are consistent with Vanzetta et al.'s findings, although our MRI could not resolve different vascular compartments. Taken together, there are strong experimental data that support CBV indeed increases slightly before CBF increases.

While these cross-modality comparisons are informative and encouraging, it is important to note that optical imaging and fMRI may not be measuring the same signal sources (arteriole, capillary, venule, or vein). fMRI measurements generally report changes in deep cortical layers, in contrast to optical imaging, which measures changes on the cortical surfaces. Our data indicate that hemodynamic changes vary with cortical depth. Thus, caution must be exercised when comparing optical and fMRI data.

Our data are in good agreement with the MRI data of Silva et al. (13), who measured CBV and BOLD at high temporal resolutions using MRI. CBF was not measured. Although the absolute times to peak were different between the two studies, as expected due to differences in stimulation durations, the relative difference in times to peak between BOLD and CBV in Silva et al.'s study (2.7 seconds – 1.9 seconds = 0.8 seconds) was essentially identical to those in our study (5.8 seconds – 5.0 seconds = 0.8 seconds) (Table 1).

Poststimulus BOLD Undershoot

Poststimulus BOLD undershoot has been widely observed. There is, however, no consensus on what causes a poststimulus BOLD undershoot. Both metabolic and hemodynamic origins of the poststimulus BOLD undershoot have been suggested. The metabolic origin hypothesis states that after stimulus is turned off, metabolism remains slightly elevated to replenish the neurotransmitter pools and other housekeeping functions after CBF has returned to baseline (29–33). The hemodynamic origin hypothesis states that venous blood volume is slow to return to baseline (balloon model (34)) after CBF has returned to baseline (24,34,35). Our results indicated that $CMRO_2$ changes remained elevated poststimulus for Layers IV–V and VI, supporting the metabolic hypothesis. Moreover, both CBF and CBV returned to baseline poststimulus, arguing against the hemodynamic hypothesis.

Earlier studies suggested that CBV levels slowly returning to baseline can cause the poststimulus BOLD undershoot, supporting the hemodynamic origin hypothesis (24,34). Some recent studies suggested that the poststimulus BOLD undershoot has a metabolic origin. For example, Tuunanen et al. (36) concluded that CBV is not elevated during poststimulus under-

shoot. Furthermore, their data demonstrated that curtailed oxygen availability (via mild hypoxia) has no effect on BOLD undershoot characteristics. These findings support the idea of a metabolic rather than hemodynamic origin for the BOLD undershoot. Similarly, Lu et al. (33) concluded that poststimulus increases in oxygen metabolism cause the BOLD undershoot using the vascular occupancy (VASO) technique. Still others suggested that both mechanisms are operative but at spatially distinct locations (29). It would not be surprising that the signal sources of the poststimulus BOLD undershoot is cortical layer-specific as well as dependent on stimulus type and duration.

Indeed, we observed that the ratio of CBF:CMRO₂ change was 3:1 for Layers I–III, whereas it was 2:1 for Layers IV–V and VI. This observation is indicative of different metabolic-vascular coupling in different cortical layer. Another potential explanation is that Layers I–III have higher vascular density, resulting in larger changes in CBF and BOLD signals. It would be of interest to investigate whether the CBF:CMRO₂ ratios also have cortical depth dependence in other brain regions.

Finally, it is important to note that CBF, CBV, and BOLD fMRI signals have very different vascular components (i.e., artery, arterioles, capillary, venules, and veins) and MRI does not have the spatial resolution to resolve these different vascular compartments. For example, CBF fMRI signal change is presumably arterial, depending on postlabeling delays (37). MION CBV fMRI signal change appears to be mostly from arterial or arteriole vessels (38). BOLD fMRI signal is mostly from venules and veins at 4.7T. The temporal dynamics could provide qualitative insights into the different vascular contributions and spatial specificity of these complicated brain-mapping fMRI signals. Indeed, the onset times reported herein are consistent with the interpretations that MION CBV signal is largely from the actively dilating arterioles, followed closely by CBF signal. BOLD signal, which lagged behind both CBV and CBF signals significantly, is mostly from venules and veins.

These results have implications in the biophysical modeling of the BOLD signals and in functional brain mapping of columnar and laminar structures using hemodynamic-based fMRI techniques. The temporal dynamics of the CBF and CBV fMRI signals relative to the BOLD signals are in agreement with the capability of CBF fMRI (37) and CBV fMRI (39) to map cortical columns, whereas conventional gradient-echo BOLD fMRI appeared to be less suited to this purpose. There is also recent evidence that spin-echo BOLD and diffusion-weighted fMRI have high spatial specificity (40). The temporal dynamics of the spin-echo fMRI and the diffusion-weighted fMRI is under investigations.

In conclusion, this study reported the dynamic evolution of CBF, CBV, BOLD and estimated CMRO₂ fMRI responses with a 500-msec temporal resolution. The key contribution of this study is that CBV, CBF, and BOLD were measured at high temporal resolution from the same pixels without depth limitation using a single modality (MRI). Although small, the differences in temporal dynamics among different fMRI signals were consistently detected. Moreover, layer-specific differences

in CBF, CBV, BOLD, and estimated CMRO₂ fMRI responses were observed. Temporal latencies of these fMRI signals have the potential to provide insights into signal sources and spatial specificity.

REFERENCES

1. Raichle ME. Circulatory and metabolic correlates of brain function in normal humans. In: Plum F, editor. Handbook of physiology—the nervous system. V: Higher functions of the brain. Bethesda, MD: American Physiological Society; 1987:643–674.
2. Ogawa S, Tank DW, Menon R, Ellermann JM, Kim S-G, Merkle H, Ugurbil K. Intrinsic signal changes accompanying sensory stimulation: functional brain mapping with magnetic resonance imaging. Proc Natl Acad Sci U S A 1992;89:5951–5955.
3. Yang Y, Gu H, Stein EA. Simultaneous MRI acquisition of blood volume, blood flow, and blood oxygenation information during brain activation. Magn Reson Med 2004;52:1407–1417.
4. Huppert TJ, Hoge RD, Diamond SG, Franceschini MA, Boas DA. A temporal comparison of BOLD, ASL, and NIRS hemodynamic responses to motor stimuli in adult humans. Neuroimage 2006;29:368–382.
5. Kida I, Rothman DL, Hyder F. Dynamics of changes in blood flow, volume, and oxygenation: implications for dynamic functional magnetic resonance imaging calibration. J Cereb Blood Flow and Metab 2007;24:690–696.
6. Vanzetta I, Hildesheim R, Grinvald A. Compartment-resolved imaging of activity-dependent dynamics of cortical blood volume and oximetry. J Neurosci 2005;25:2233–2244.
7. Oldfield RC. Assessment and analysis of handedness: the Edinburgh Inventory. Neuropsychologia 1971;9:97–113.
8. Malonek D, Dirnagl U, Lindauer U, Yamada K, Kanno I, Grinvald A. Vascular imprints of neuronal activity: relationships between the dynamics of cortical blood flow, oxygenation, and volume changes following sensory stimulation. Proc Natl Acad Sci U S A 1997;94:14826–14831.
9. Jones M, Berwick J, Johnston D, Mayhew J. Concurrent optical imaging spectroscopy and laser-Doppler flowmetry: the relationship between blood flow, oxygenation, and volume in rodent barrel cortex. Neuroimage 2001;13:1002–1015.
10. Jones M, Berwick J, Mayhew J. Changes in blood flow, oxygenation, and volume following extended stimulation of rodent barrel cortex. Neuroimage 2002;15:474–487.
11. Sheth SA, Nemoto M, Guioiu MW, Walker MA, Toga AW. Spatiotemporal evolution of functional hemodynamic changes and their relationship to neuronal activity. J Cereb Blood Flow Metab 2005;25:830–841.
12. Mandeville JB, Marota JJ, Kosofsky BE, Keltner JR, Weissleder R, Rosen BR. Dynamic functional imaging of relative cerebral blood volume during rat forepaw stimulation. Magn Reson Med 1998;39:615–624.
13. Silva AC, Koretsky AP, Kellman P, Duyn JH. fMRI impulse response for BOLD and CBV contrast in rat somatosensory cortex. In: Proc ISMRM, Kyoto, Japan; 2004:277.
14. Liu ZM, Schmidt KF, Sicard KM, Duong TQ. Imaging oxygen consumption in forepaw somatosensory stimulation in rats under isoflurane anesthesia. Magn Reson Med 2004;52:277–285.
15. Sicard KM, Duong TQ. Effects of hypoxia, hyperoxia and hypercapnia on baseline and stimulus-evoked BOLD, CBF and CMRO₂ in spontaneously breathing animals. Neuroimage 2005;25:850–858.
16. Shen Q, Ren H, Cheng H, Fisher M, Duong TQ. Functional, perfusion and diffusion MRI of acute focal ischemic brain injury. J Cereb Blood Flow Metab 2005;25:1265–1279.
17. Silva AC, Kim S-G. Pseudo-continuous arterial spin labeling technique for measuring CBF dynamics with high temporal resolution. Magn Reson Med 1999;42:425–429.
18. Davis TL, Kwong KK, Weisskoff RM, Rosen BR. Calibrated functional MRI: mapping the dynamics of oxidative metabolism. Proc Natl Acad Sci U S A 1998;95:1834–1839.
19. Hoge RD, Atkinson J, Gill B, Crelier GR, Marrett S, Pike GB. Linear coupling between cerebral blood flow and oxygen consumption in activated human cortex. Proc Natl Acad Sci U S A 1999;96:9403–9408.
20. Silva AC, Lee S-P, Iadecola C, Kim S-G. Early temporal characteristics of CBF and deoxyhemoglobin changes during somatosensory stimulation. J Cereb Blood Flow Metab 2000;20:201–206.

21. Mandeville JB, Marota JJ. Vascular filters of functional MRI: spatial localization using BOLD and CBV contrast. *Magn Reson Med* 1999;42:591–598.
22. Masamota K, Kim T, Fukuda M, Wang P, Kim S-G. Relationship between neural, vascular, and BOLD signals in isoflurane-anesthetized rat somatosensory cortex. *Cereb Cortex* 2007;17:942–950.
23. Duong TQ, Silva AC, Lee S-P, Kim S-G. Functional MRI of calcium-dependent synaptic activity: cross correlation with CBF and BOLD measurements. *Magn Reson Med* 2000;43:383–392.
24. Mandeville JB, Marota JJ, Ayata C, Moskowitz MA, Weisskoff RM, Rosen BR. MRI measurement of the temporal evolution of relative CMRO2 during rat forepaw stimulation. *Magn Reson Med* 1999;42:944–951.
25. Boxerman JL, Hamberg LM, Rosen BR, Weisskoff RM. MR contrast due to intravascular magnetic susceptibility perturbations. *Magn Reson Med* 1995;34:555–566.
26. Silva AC, Koretsky AP. Laminar specificity of functional MRI onset times during somatosensory stimulation in rat. *Proc Natl Acad Sci U S A* 2002;99:15182–15187.
27. Wu G, Luo F, Li Z, Zhao X, Li SJ. Transient relationships among BOLD, CBV, and CBF changes in rat brain as detected by functional MRI. *Magn Reson Med* 2002;48:987–993.
28. Uludag K, Dubowitz DJ, Yoder EJ, Restom K, Liu TT, Buxton RB. Coupling of cerebral blood flow and oxygen consumption during physiological activation and deactivation measured with fMRI. *Neuroimage* 2004;23:148–155.
29. Yacoub E, Ugurbil K, Harel N. The spatial dependence of the post-stimulus undershoot as revealed by high-resolution BOLD- and CBV-weighted fMRI. *J Cereb Blood Flow and Metab* 2006;26:634–644.
30. Frahm J, Kruger KD, Merboldt KD, Kleinschmidt A. Dynamic uncoupling and recoupling of perfusion and oxidative metabolism during focal brain activation in man. *Magn Reson Med* 1996;35:143–148.
31. Kruger G, Kleinschmidt A, Frahm J. Dynamic MRI sensitized to cerebral blood oxygenation and flow during sustained activation of human visual cortex. *Magn Reson Med* 1996;35:797–800.
32. Ances BM, Buerk DG, Greenberg JH, Detre JA. Temporal dynamics of the partial pressure of brain tissue oxygen during functional forepaw stimulation in rats. *Neurosci Lett* 2001;306:106–110.
33. Lu H, Golay X, Pekar JJ, Van Zijl PC. Sustained poststimulus elevation in cerebral oxygen utilization after vascular recovery. *J Cereb Blood Flow and Metab* 2004;24:764–770.
34. Buxton RB, Wong EC, Frank LR. Dynamics of blood flow and oxygenation changes during brain activation: the balloon model. *Magn Reson Med* 1998;39:855–864.
35. Mandeville JB, Marota JJ, Ayata C, et al. Evidence of a cerebrovascular postarteriole windkessel with delayed compliance. *J Cereb Blood Flow Metab* 1999;19:679–689.
36. Tuunanen PI, Vidyasagar R, Kauppinen RA. Effects of mild hypoxic hypoxia on poststimulus undershoot of blood-oxygenation-level-dependent fMRI signal in the human visual cortex. *Magn Reson Imag* 2006;24:993–999.
37. Duong TQ, Kim D-S, Ugurbil K, Kim S-G. Localized blood flow response at sub-millimeter columnar resolution. *Proc Natl Acad Sci U S A* 2001;98:10904–10909.
38. Kim T, Hendrich KS, Masamoto K, Kim SG. Arterial versus total blood volume changes during neural activity-induced cerebral blood flow change: implication for BOLD fMRI. *J Cereb Blood Flow Metab* 2007;27:1235–1247.
39. Zhao F, Wang P, Hendrich K, Kim SG. Spatial specificity of cerebral blood volume-weighted fMRI responses at columnar resolution. *Neuroimage* 2005;27:416–424.
40. Duong TQ, Yacoub E, Adriany G, et al. Microvascular BOLD contribution at 4 and 7 T in human brain: gradient echo and spin echo fMRI with suppression of blood effects. *Magn Reson Med* 2003;49:1019–1027.